Physica A 593 (2022) 126961

Contents lists available at ScienceDirect

Physica A

journal homepage: www.elsevier.com/locate/physa

Development of travel time functions for disrupted urban arterials with microscopic traffic simulation

Guangyang Hou [a], Suren Chen [a,*], Yulong Bao [b]

[a] Department of Civil & Environmental Eng., Colorado State University, Fort Collins, CO 80523, United States of America
[b] Department of Bridge Engineering, Southwest Jiaotong University, Chengdu 610031, Sichuan, PR China

ARTICLE INFO

Article history:
Received 1 May 2021
Received in revised form 13 January 2022
Available online 25 January 2022

Keywords:
Partially blocked road
Travel time function
Cellular automaton
Traffic simulation

ABSTRACT

Urban traffic networks consisting of partially blocked roads often need to remain open to traffic before, during and after disasters because of their vital roles to hazard preparation, emergency response and recovery of urban communities. To conduct effective traffic planning of disrupted transportation networks highly depends on accurate prediction of travel time on partially blocked roads, which is very different from that on intact roads. Due to the lack of appropriate models, travel time prediction approaches developed for intact roads have often been directly applied to partially blocked roads, leading to inaccurate travel time estimates. Unrealistic travel time estimates of partially blocked roads as well as the whole transportation network further affect traffic planning, emergency response and other decision-makings which are heavily reliant on travel time prediction. A new approach to develop travel time functions for partially blocked roads in urban areas is proposed to close this gap based on microscopic traffic simulation. First, an improved model for simulating traffic on partially blocked roads is developed by extending the existing cellular automaton model. Second, the improved traffic model is validated at microscopic and macroscopic levels with measured traffic data from an urban road. Third, traffic simulations under various scenarios with different demand flow rates, truck ratios and blockage ratios are conducted through microscopic simulation experiments. Finally, a set of continuous traffic time functions are further developed for disrupted traffic flow with parameters estimated from the generated traffic data. The developed travel time functions for a typical urban arterial road are then compared with the standard Bureau of Public Roads function. The comparison suggests that the standard Bureau of Public Roads function would considerably underestimate the travel time on partially blocked roads and the proposed travel time functions can offer a more realistic prediction. The proposed methodology of developing the travel time functions of partially blocked roads will be helpful for accurate estimation of traffic demand of post-hazard transportation networks.

1. Introduction

Transportation networks are critical for post-disaster evacuation, emergency response and long-time recovery activities. Road networks are easily disrupted during or following some hazards, such as by damaged bridges and roadways, fallen trees and utility facilities, and debris from nearby damaged buildings, etc. In the emergency response phase,

* Corresponding author.
E-mail addresses: guangyang.hou@colostate.edu (G. Hou), suren.chen@colostate.edu (S. Chen), baoyulong1991@163.com (Y. Bao).

https://doi.org/10.1016/j.physa.2022.126961
0378-4371/

disrupted roads with full or partial closure might prevent access to the impacted areas, causing delay in rescue and relief operations. In the recovery stage, the restoration of other lifeline infrastructures, such as electrical network, water supply network and telecommunication network, may also be affected by extra travel delay on disrupted roads.

Travel time function or volume delay function describes the relationship between travel time and traffic volume on a road link. In traffic demand modeling, travel time is usually treated as cost, which directly influences the route choices of travelers. Travel time function, as a sub-model of static traffic assignment procedure, plays a very important role in traffic demand modeling and the Bureau of Public Roads (BPR) function is one of the most widely used travel time functions [1]. Despite reduced traffic capacity, partially blocked roads (PBR) of some critical urban traffic networks often remain open to traffic before, during and after many hazards. To conduct effective traffic planning of road networks involving PBR highly depends on accurate prediction of travel time on PBR, which is very different from those on intact roads. Because there is so far no available travel time function for PBR, the standard BPR function for intact roads has been often adopted by simply applying the reduced capacity for post-hazard transportation demand modeling. However, not only the traffic capacity is reduced for PBR, but also the travel time–volume relationship has significantly changed from its normal condition because of the interaction between vehicles and obstructions. Thus, the standard BPR function will likely give inaccurate travel time prediction on PBR, which may lead to erratic results in the post-hazard transportation network analysis. So, there is great need to develop travel time functions for PBR that reflect the relationship between travel time and demand flow rate realistically.

The primary objective of the study is to develop a methodology to predict the travel time functions for PBR in urban areas based on microscopic traffic simulation. Firstly, an improved cellular automaton (CA) model for traffic flow simulation on disrupted urban arterials is proposed based on the two-lane safety driving (SD) model, with which unrealistic deceleration behaviors can be avoided and driver's behaviors during traffic signal change intervals can be realistically replicated. Secondly, the proposed model is calibrated and validated at microscopic and macroscopic levels with measured traffic data from an urban road in Colorado. Finally, traffic data under various scenarios with different demand flow rates, truck ratios and blockage ratios are generated through microscopic simulation experiments. A continuous traffic time function is then developed for disrupted traffic flow and its parameters are estimated with the generated traffic data. The primary contributions of this paper include (1) an improved CA model for traffic simulation on PBR, and (2) a continuous travel time function that can consider the combined effect of demand flow rate, truck ratio and blockage ratio, which is calibrated with travel time data generated through microscopic simulation experiments. The PBR travel time functions, developed for the first time, will be helpful for accurate travel demand estimates in post-hazard transportation network analysis.

The rest of this paper is organized as follows. Firstly, related existing works from the literature are reviewed; next section is to introduce the proposed traffic simulation model, followed by the model calibration and validation; the following section describes the process to develop travel time functions for PBR; and finally, the conclusions are summarized.

2. Literature review

Travel time functions are usually developed based on measured or simulated traffic data. It is a traditional approach to estimate travel time functions by calibrating empirical travel time models based on observed traffic data, which can be collected with various techniques, such as floating car, license plate matching, ITS probe vehicle, loop detector and radar. In addition to the well-known Bureau of Public Roads (BPR) function [1], there are other empirical travel time estimate models, such as conical travel time function [2], Akcelik model [3], Singapore model [4], Skabardonis–Dowling model [5] and HCM formula [6], which were developed to better reflect observed operating conditions and road facility characteristics. However, all these models were developed with traffic data of intact roads, and none of them is suitable for travel time prediction on partially blocked roads due to the unique characteristics of disrupted traffic flow on these roads.

Accounting for a considerable portion of urban traffic, trucks in heterogeneous traffic flow often significantly contribute to traffic delay due to their different sizes, travel speeds, mechanical properties, and headways from cars. Previous studies indicate that the flow rate and speed decrease with the increase of the truck ratio [7]. The standard BPR function does not reflect the effect of traffic flow heterogeneity caused by different vehicle types on traffic congestion. The conversion of trucks into cars by using the passenger car equivalent method only recognizes the size difference but ignores the operational difference between those vehicle types. Truck's impact on the traffic time function has been included in only some existing studies [8–10].

Blockage size is another factor that affects the performance of PBR, which has been preliminarily considered in existing studies. For example, lateral and longitudinal blockage sizes have been incorporated in the empirical equations to calculate the remaining traffic capacity [11]. Blockage size (e.g., work zone length) has been found to directly influence the travel time required for a vehicle to transverse a road [12]. Given various possible blockage scenarios following different hazards, incorporating the effect of the blockage size in travel time function can be challenging, but crucial for rationally evaluating the post-hazard performance of disrupted transportation networks by considering the interaction between roads and other interdependent infrastructures. However, there is no existing travel time function that includes the effect of blockage size.

Several studies have considered the impact of PBR in the post-hazard urban transportation network analysis, most of which focused on the connectivity analysis of disrupted transportation networks with fully- and partially-closed

roads [13–15]. Only a few studies considered the effect of PBR on traffic delay by modeling the post-hazard traffic demand. Tamima and Chouinard [16] evaluated system vulnerability of transportation networks after earthquakes and considered road closure due to fallen debris from damaged buildings. The reduced capacity of PBR was estimated by assuming there is a linear relationship between the remaining capacity and the percentage of the road width being covered by debris. However, the travel time on PBR in this study was calculated by the standard BPR function including the normal free-flow time and reduced capacity rather than realistic travel time functions for disrupted scenarios of PBR.

Despite the essential role of travel time prediction of PBR for the resiliency analysis of disrupted transportation networks, extensive literature review has not identified any published literature regarding travel time functions of PBR. One big challenge for developing travel time functions of PBR is the lack of real-world traffic data. As a result, microscopic traffic simulation has become a good alternative. Among those existing microscopic traffic simulation models, cellular automaton (CA) model is one of the most widely used models, thanks to its high efficiency and flexibility [17]. Many existing studies investigated the disrupted traffic flow on PBR induced by tollbooths, accidents, lane reduction, and work zone with CA models [18–27].

Despite recent effort towards realistic simulation of disrupted traffic, one major challenge for CA-based traffic flow simulation is about unrealistic deceleration behavior. There are generally two types of unrealistic deceleration behavior in existing CA models for disrupted traffic. Firstly, when a vehicle approaches a static obstruction or traffic jam, it may make a sudden stop by sharply reducing its maximum velocity to avoid a rear-end crash. In this situation, the required deceleration rate is much higher than the mechanical deceleration capability by most vehicles, making the deceleration rate unrealistic. This is caused by some limitations of most existing models: vehicle's velocity is determined only by the gap between itself and its preceding vehicle, and vehicles tend to brake abruptly at the last second. Secondly, on a disrupted road, when a vehicle enters the merging area before an obstruction, it usually decelerates gradually to a safe speed (e.g., posted reduced speed limit). However, such a deceleration process in existing CA models would be completed within 1 s regardless, which may lead to an unrealistically high deceleration rate. Although unrealistic driving behavior may still lead to reasonable long-term averaged cumulative outcome for normal traffic flow, it may cause erratic detailed results for disrupted traffic flow which are important for PBR performance. Lan et al. [28] improved the CA model with piecewise-linear speed variation to avoid the first type of unrealistic deceleration behaviors in the work zone traffic simulation. However, the second type of unrealistic deceleration behavior still existed in their model. Therefore, a general CA-based model for simulation of disrupted traffic flow that can fully consider realistic deceleration driving behavior is still needed.

The literature review also suggests that existing studies related to travel time functions mainly focused on normal traffic and very few studies had examined the development of travel time functions on PBR. In the meantime, the impact of trucks on travel time under normal conditions has been studied previously, but the effect of blockage size also needs to be incorporated when estimating travel time on PBR. Moreover, existing CA-based traffic simulation models need to be improved to fully consider realistic deceleration driving behavior. This study aims to overcome these limitations and propose a new methodology to develop the travel time functions of PBR in urban areas through microscopic traffic simulation.

3. Formulation of microscopic traffic simulation model

3.1. A typical PBR scenario

For urban transportation systems in the US, four-lane arterials (i.e., two lanes in each direction) and two-lane arterials (i.e., one lane in each direction) are the most popular arterial types. If one lane of a two-lane arterial is blocked, there will be no traffic in that direction unless manual traffic intervention is applied, such as alternating one-way traffic for both directions. Such a scenario involves very low traffic capacity and is beyond the scope of the present study. This study will focus on the two-lane traffic in each direction on four-lane arterials. Depending on the specific hazard and surrounding environment, road links can be blocked in many ways. Traffic performance of a PBR is determined by the specific blockage scenario. One of the most common blockage scenarios for two-lane traffic is that one lane is partially closed, and the other lane is open to traffic, which is like the two-lane traffic with a work zone, as shown in Fig. 1. Although there are other more complicated blockage scenarios, this study will focus on the most typical disruptive scenario in Fig. 1. This is because other blockage scenarios either lead to full closure (e.g., multiple blockages near to each other) or can be simplified into the scenario being studied here (e.g., multiple blockages far apart).

As shown in Fig. 1, a blocked area with a length of L_b is included in the road section. A warning sign is usually placed at the upstream of the blockage showing how far ahead of the lane is closed, often accompanied by reduced speed limit. The area between the warning sign and the blocked area is called merging area with the length of L_m, where drivers on the blocked lane will try to switch lane to the adjacent lane. In the meantime, vehicles often need to slow down to the reduced speed limit before moving into the blocked area. Any area beyond the blocked and merging areas is called normal area.

In some situations, warning signs may not be immediately available following an incident or a hazard before the traffic management is implemented. In this situation, the length of the merging area and reduced speed limit will depend on individual drivers and traffic conditions. Due to different driving behavior, timid drivers may merge lane far before the

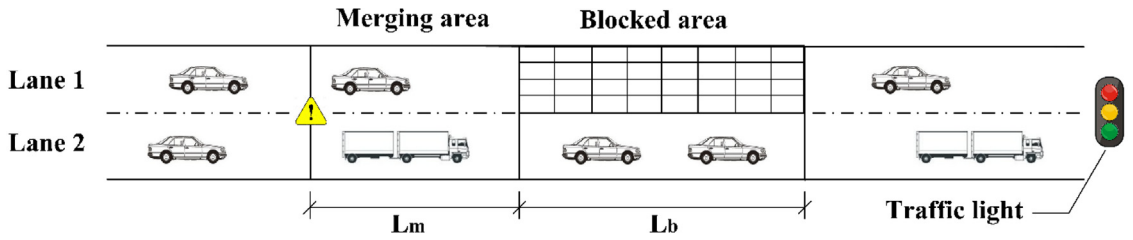

Fig. 1. Schematic diagram of a road section with a blockage.

blockage and drive slowly in the blocked area, while aggressive drivers may begin to merge lane very late and drive relatively fast.

As shown in Fig. 1, vehicles enter the road section from the left end of the figure and there is a traffic light at the right end with the cycle length of T. The durations of green-light, yellow-light, and red-light phases are T_g, T_y and T_r, respectively. If a vehicle reaches the right end of the road section, it will leave when the traffic light is green and stop when the traffic light is red. During a change interval, drivers will stop or proceed through the intersection depending on the distance to the intersection and the driving speed.

3.2. CA-based model

To avoid unrealistic deceleration behavior mentioned in Section 1, an improved CA model is proposed for heterogeneous traffic flow on partially blocked urban roads by extending the two-lane safety driving (SD) model [7]. The SD model is known for its ability to fully avoid unrealistic deceleration behaviors in traffic simulation. Because vehicles on partially blocked roads experience frequent deceleration, the SD model is needed to realistically simulate this type of disrupted traffic. The original SD model was developed for simulation of normal traffic on highways. Through the extension, the improved CA model can simulate traffic not only on PBR but also on urban arterials with traffic lights. In this model, the lanes are discretized into many identical cells. Each cell is either empty or occupied by a vehicle at a time. Depending on the length of each individual vehicle, different numbers of cells may be occupied by each vehicle. The vehicle velocity is an integer varying from 0 to v_{max}, which is the maximum velocity of a vehicle. At each time step, the position and velocity of each vehicle are updated through the forwarding rule and lane-changing rule.

Open boundary conditions are used in this model. Vehicles enter the road section from the left end with a flow rate of q, and the time headway h is assumed to follow a displaced exponential distribution, which has a cumulative probability distribution $F(h) = 1 - e^{-\lambda(h-t_m)}$, where t_m is the minimum headway between vehicles and $\lambda = q/(1 - t_m q)$. We assume that the position of the left-most vehicle is x_{last}, and the maximum velocity and length of the new vehicle n are $v_{n,max}$ and l_n, respectively. If $x_{last} > v_{n,max} + l_n$ and vehicle n meets the time headway condition, it will enter the system at the position of $x_n = min\left(x_{last} - l_n - v_{n,max}, v_{n,max}\right)$ with a velocity of $v_{n,max}$.

3.2.1. Forwarding rule in the green-light phase

During different traffic light phases, drivers have different driving behavior so the forwarding rules in the CA model are also different. Therefore, forwarding rules in the green-light phase, and yellow and red-light phase are introduced. There are four consecutive steps in the forwarding rules during the green-light phase, which are performed in parallel for all vehicles.

S1: Safe distance. Obtain three safe distances for vehicle n, including safe acceleration distance d_{acc_n}, safe keep velocity distance d_{keep_n} and safe deceleration distance d_{dec_n}. To safely accelerate, keep a velocity, or decelerate, a vehicle must maintain a safe following distance with its preceding vehicle, d_{acc_n}, d_{keep_n}, or d_{dec_n}, respectively. The worst possible scenario is assumed to calculate those distances: the preceding vehicle begins to brake with the maximum deceleration rate at time step t and the following vehicle may accelerate, keep its velocity, or decelerate at time step t, and begins to brake with the maximum deceleration rate at time step $t + 1$. If the distance the following and preceding vehicles have travel until they stop are s_{n+1} and s_n, respectively, the difference of the travel distances between the two vehicles $s_n - s_{n+1}$ is deemed the safe distance to avoid a collision. This provides the basis for calculating those three safe distances for typical car–car cases with Eqs. (1)–(3). However, the basic algorithm will not work when the preceding and following vehicles have vastly different maximum deceleration rates, for example a truck being the proceeding vehicle and a passenger car being the following vehicle in heterogeneous traffic. Therefore, the three safe distances for special car-truck cases are obtained by Eqs. (4)–(6), which are modified from Eqs. (1)–(3). Detailed explanations of Eqs. (1)–(6) can be found in Refs. [7,29]. When a vehicle approaches a stationary obstacle, the driver will accelerate, keep its velocity, or decelerate according to the distance from the obstacle. Similarly, the three safe distances for the vehicle-obstacle cases can be calculated by Eqs. (7)–(9), which are also modified from Eqs. (1)–(3).

For the typical car–car cases, where vehicle $n+1$ is followed by vehicle n, d_{acc_n}, d_{keep_n} and d_{dec_n} are obtained with the following equations:

$$d_{acc_n} = max\left(0, \sum_{i=0}^{(v_n(t)+a)_{divM_n}} [(v_n(t)+a) - iM_n] - \sum_{i=0}^{(v_{n+1}(t)-M_{n+1})_{divM_{n+1}}} [(v_{n+1}(t)-M_{n+1}) - iM_{n+1}]\right) \tag{1}$$

$$d_{keep_n} = max\left(0, \sum_{i=0}^{v_n(t)_{divM_n}} [v_n(t) - iM_n] - \sum_{i=0}^{(v_{n+1}(t)-M_{n+1})_{divM_{n+1}}} [(v_{n+1}(t)-M_{n+1}) - iM_{n+1}]\right) \tag{2}$$

$$d_{dec_n} = max\left(0, \sum_{i=0}^{(v_n(t)-d)_{divM_n}} [(v_n(t)-d) - iM_n] - \sum_{i=0}^{(v_{n+1}(t)-M_{n+1})_{divM_{n+1}}} [(v_{n+1}(t)-M_{n+1}) - iM_{n+1}]\right) \tag{3}$$

For special car-truck cases, when both the velocity $v_n(t)$ and limited deceleration capability M_n of vehicle n (car) are higher than $v_{n+1}(t)$ and M_{n+1} of the leading vehicle $n+1$ (truck), d_{acc_n}, d_{keep_n} and d_{dec_n} are calculated with the following equations.

For d_{acc_n}, we set $\Delta v = v_{n+1}(t) - M_{n+1} - (v_n(t)+a)$, $\Delta M = M_{n+1} - M_n$, $\tau_1 = \Delta v_{div\Delta M}$, $\tau_2 = (v_n(t)+a)_{divM_n}$. In Eq. (4), τ_1 and τ_2 are two special time instants, at which the local minimum space gap between the two vehicles is reached. The smaller of the two space gaps calculated with τ_1 and τ_2 is deemed as the safe acceleration distance of the following car. The detailed derivation is not given for the sake of brevity. However, this information is available in Li et al. [7]. It is noted that τ_1 and τ_2 have the similar meaning in the following Eqs. (5) and (6).

$$d_{acc_n} = min\left\{\sum_{i=0}^{\tau_1 \ or \ \tau_2} [((v_n(t)+a) - iM_n) - ((v_{n+1}(t) - M_{n+1}) - iM_{n+1})]\right\} \tag{4}$$

For d_{keep_n}, we set $\Delta v = v_{n+1}(t) - M_{n+1} - v_n(t)$, $\Delta M = M_{n+1} - M_n$, $\tau_1 = \Delta v_{div\Delta M}$, $\tau_2 = v_n(t)_{divM_n}$.

$$d_{keep_n} = min\left\{\sum_{i=0}^{\tau_1 or \tau_2} [(v_n(t) - iM_n) - ((v_{n+1}(t) - M_{n+1}) - iM_{n+1})]\right\} \tag{5}$$

For d_{dec_n}, we set $\Delta v = v_{n+1}(t) - M_{n+1} - (v_n(t) - d)$, $\Delta M = M_{n+1} - M_n$, $\tau_1 = \Delta v_{div\Delta M}$, $\tau_2 = (v_n(t) - d)_{divM_n}$.

$$d_{dec_n} = min\left\{\sum_{i=0}^{\tau_1 or \tau_2} [((v_n(t) - d) - iM_n) - ((v_{n+1}(t) - M_{n+1}) - iM_{n+1})]\right\} \tag{6}$$

For vehicle-obstacle cases, where vehicle n is the nearest vehicle behind an obstacle, d_{acc_n}, d_{keep_n} and d_{dec_n} are calculated with the following equations:

$$d_{acc_n} = max\left(0, \sum_{i=0}^{(v_n(t)+a)_{divM_n}} [(v_n(t)+a) - iM_n]\right) \tag{7}$$

$$d_{keep_n} = max\left(0, \sum_{i=0}^{v_n(t)_{divM_n}} [v_n(t) - iM_n]\right) \tag{8}$$

$$d_{dec_n} = max\left(0, \sum_{i=0}^{(v_n(t)-d)_{divM_n}} [(v_n(t)-d) - iM_n]\right) \tag{9}$$

S2: Slow to accelerate. Determine the stochastic noise parameter R_a based on the vehicle's velocity $v_n(t)$.

$$R_a = min\left(R_d, R_0 + v_n(t) \cdot (R_d - R_0)/v_s\right) \tag{10}$$

S3: Update the velocities of all vehicles simultaneously by comparing the vehicle's space gap $d_n(t)$ with the calculated three safe distances. When vehicles approach the merging area, they need to decelerate to the reduced speed limit v_r gradually in a short time and obey the speed limit until moving out of the blocked area. At the same time, in the merging area, vehicles in the blocked lane (lane 1) will try to change to the unblocked lane (lane 2) as soon as possible. Therefore, the forwarding rules in the merging and blocked areas are different from those in the normal area.

S3a: Acceleration.

In the normal area, where the maximum velocity is v_{max}, if $d_n(t) \geq d_{acc_n}$, or in the merging and blocked areas, where the maximum velocity is v_r, if $d_n(t) \geq d_{acc_n}$ and $v_n(t) \leq v_r$

$$v_n(t+1) = \begin{cases} min\left(v_n(t) + a, v_{max} \text{ or } v_r\right), \text{ if } randf() \leq (R_a) \\ v_n(t), \text{ otherwise} \end{cases} \tag{11}$$

S3b: Random slowing down.

In the normal area, if $d_{acc_n} > d_n(t) \geq d_{keep_n}$, or in the merging and blocked areas, if $d_{acc_n} > d_n(t) \geq d_{keep_n}$ and $v_n(t) \leq v_{wz}$

$$v_n(t+1) = \begin{cases} max\left(v_n(t) - d, 0\right), \text{ if } randf() \leq (R_s) \\ v_n(t), \text{ otherwise} \end{cases} \tag{12}$$

S3c: Braking.

In the normal area, if $d_{keep_n} > d_n(t) \geq d_{dec_n}$,

$$v_n(t+1) \rightarrow max\left(v_n(t) - d, 0\right) \tag{13}$$

In the merging and blocked areas,

$$v_n(t+1) = \begin{cases} max\left(v_n(t) - d, 0\right), \text{ if } v_n(t) \leq v_r \text{ and } d_{keep_n} > d_n(t) \geq d_{dec_n} \\ max\left(v_n(t) - d, 0\right), \text{ if } v_n(t) > v_r \text{ and } d_n(t) \geq d_{dec_n} \\ v_n(t), \text{ otherwise} \end{cases} \tag{14}$$

S3d: Emergency braking. If $v_n(t) > 0$ and $d_n(t) < d_{dec_n}$,

$$v_n(t+1) \rightarrow max\left(v_n(t) - M_n, 0\right) \tag{15}$$

S4: Vehicle movement.

$$x_n(t+1) \rightarrow x_n(t) + v_n(t+1) \tag{16}$$

Here, $x_n(t)$ and $v_n(t)$ denote the longitudinal position and velocity of vehicle n at time step t, respectively; $d_n(t)$ denotes the space gap of vehicle n, which is the clear distance between vehicle n and its preceding vehicle $n+1$ on the current lane, $d_n(t) = x_{n+1} - x_n - l_n$; if vehicle n is the first vehicle on its lane, a large value will be assigned to $d_n(t)$; l_n denotes the length of vehicle n; a and d denote the normal acceleration and deceleration rates, respectively; M_n denotes the limited deceleration rate of vehicle n; X_{divY} denotes the integer division, which is defined as $X_{divY} = [X/Y]$, where "/" denotes normal division and $[z]$ is the floor function; v_s is a constant velocity slightly above 0; R_0 and R_d are given constants that control the velocity fluctuations of vehicles, $0 < R_0 < R_d \leq 1$; $R_a = R_0$ when the $v_n(t) = 0$, and $R_a = R_d$ when $v_n(t) \geq v_s$; R_s is the slowing down probability.

3.2.2. Forwarding rule in yellow and red-light phase

Once the yellow light is on, drivers must decide to stop or to cross the intersection. Therefore, at the onset of yellow light, the status of a vehicle needs to be determined based on the vehicle's distance to the intersection and the driving speed. There are three possible statuses for each vehicle, namely "cross status", "stop status" and "follow status". A vehicle with a cross status will cross the intersection during the yellow-light phase. With a stop status, the vehicle will stop in front of the intersection during the yellow and red-light phases. There is only one vehicle with a stop status on each lane. All the vehicles behind any vehicle in "stop status" are in "follow status", which will move by following their preceding vehicles. A vehicle's status will be determined by three algorithms in the proposed CA model. The first algorithm is used to reflect the uncertainty of a driver's decision with a distance-dependent stopping probability function. A logistic function adopted by Hsu and Chiou [30] is used to compute the probability of stop decision of a vehicle at the onset of yellow light, as expressed in Eq. (17). The logistic function describes the relationship between the stopping probability of a vehicle and its distance to the intersection. Generally, as the distance to the intersection decreases, the stopping probability increases.

$$P_s = \frac{1}{1 + e^{-\alpha(d_{sig} - \beta)}} \tag{17}$$

where P_s is the stopping probability of a vehicle; d_{sig} is the distance to the intersection; α and β are two shape parameters.

The second algorithm is that if a vehicle cannot stop in front of the intersection during the yellow-light phase by decelerating from its current speed with the maximum deceleration rate, it will have a "cross status". If not, the vehicle may have a "stop status". The stopping distance during the yellow-light phase can be expressed with Eqs. (18) and (19).

$$t_d = v_n(t)_{div\ M_n} \tag{18}$$

```
if S_d ≤ d_sig
    if rand() ≥ P_s
        st(i) = 2
    else
        if S_c ≤ d_sig
            st(i) = 2
        else
            st(i) = 1
        end
    end
else
    st(i) = 1
end
```

Fig. 2. Logic algorithm for vehicle status determination.

$$S_d = \begin{cases} \sum_{i=1}^{t_d} \left[v_n(t) - iM_n \right], \text{if } t_d \le t_y \\ \sum_{i=1}^{t_y} \left[v_n(t) - iM_n \right], \text{if } t_d > t_y \end{cases} \tag{19}$$

The third algorithm is that if a vehicle driver decides to proceed through the intersection but cannot reach the intersection by accelerating with the normal deceleration rate, the vehicle will have a "stop status" when it reaches the intersection. The driving distance during the yellow-light phase can be expressed as Eqs. (20) and (21).

$$t_c = (v_{max} - v_n(t))_{div\ a} \tag{20}$$

$$S_c = \begin{cases} \sum_{i=1}^{t_c} \left[v_n(t) - ia \right] + \left(t_y - t_c \right) v_{max}, \text{if } t_c \le t_y \\ \sum_{i=1}^{t_y} \left[v_n(t) - ia \right], \text{if } t_c > t_y \end{cases} \tag{21}$$

We set the identifier of "stop status", "cross status" and "follow status" as $st = 2, 1, and\ 0$, respectively. The "stop status" and "cross status" will be firstly determined by the logic algorithm displayed in Fig. 2 by considering all three above-mentioned conditions. The algorithm will be checked for all the vehicles from the first to the last one on each lane. Once the vehicles with "stop status" and "cross status" are identified, the statuses of the rest vehicles will be assigned accordingly.

After the vehicle statuses are all identified, vehicles with different statuses will move by following different forwarding rules. Forwarding rules used in the green-light phase will still apply to vehicles with a "cross status" and "follow status". However, those forwarding rules will need some revisions before applying to vehicles with "stop status". Firstly, three safe distances in step S1, including safe acceleration distance d_{acc_n}, safe keep velocity distance d_{keep_n} and safe deceleration distance d_{dec_n}, will be calculated with Eqs. (7) to (9), respectively. Secondly, in step S3, space gap $d_n(t)$ will be substituted with $d_{sig}(t)$.

3.2.3. Lane-changing rule

The symmetric lane-changing rules are adopted in this model with the incentive and safety criteria. Once the lane-changing rules are satisfied, a vehicle will perform lane-changing maneuver with a probability of R_c. Vehicles in different areas have different lane-changing behavior: vehicles in the blocked area cannot change lane; moreover, vehicles in the merging area will try to switch from lane 1 to lane 2 but are not allowed to switch lane from lane 2 to lane 1. Therefore, different lane-changing rules will be applied depending on which area any vehicle is currently in. In the normal area, the incentive and safety criterion of lane change can be expressed by Eqs. (22) and (23), respectively.

$$d_n < d_{acc_n} \text{ and } d_{n,other} \ge d_{acc_{n,other}} \tag{22}$$

$$d_{n,back} > d_{dec_{back,n}} \tag{23}$$

Table 1
Characteristics of the studied road segment.

Characteristics	Value
Name	Drake
Type	Urban arterial
Direction	Eastbound
Lane number	2
Lane width	3.5 m
Shoulder bikeway width	1.5 m
Speed limit	18 m/s (40 mph)
Length	1610 m
Work zone length	435 m
Warning sign location	300 m upstream

where $d_{n,other}$ denotes the gap between vehicle n and the nearest vehicle in front of it in the adjacent lane, i.e., the front vehicle; $d_{n,back}$ denotes the gap between vehicle n and the nearest vehicle behind it in the adjacent lane, i.e., the back vehicle; $d_{acc_{n,other}}$ denotes the safe acceleration distance of vehicle n if it switches to the adjacent lane; $d_{dec_{back,n}}$ denotes the safe deceleration distance of the back vehicle if vehicle n is switched to the adjacent lane.

Because vehicles in the merging area will try hard to switch from lane 1 to lane 2, the incentive criterion of lane change for them becomes less strict than that of vehicles in the normal area. Therefore, the incentive criterion is modified as follows.

$$d_{n,other} \geq d_{dec_{n,other}} \tag{24}$$

where $d_{dec_{n,other}}$ denotes the safe deceleration distance of vehicle n if it switches to the adjacent lane. The safety criterion of lane change is the same as that in the normal area. Besides, vehicles in lane 2 will not change lane in the advance warning area, and therefore the lane-changing probability is set as $R_c = 0$.

4. Model calibration and validation

4.1. Data collection

The data used in this study was collected from Drake Road between Shields Street and Taft Hill Road, a two-lane arterial road in the City of Fort Collins, Colorado. There are two reasons why this road was chosen. Firstly, there was a work zone area on one of the two lanes on this road, which can be treated as a typical PBR scenario. Secondly, there was a data collection system Bluetoad installed on both ends of the road. The total length of the road is 1610 m with the speed limit of 18 m/s (40 mph). The work zone was located from 644 to 1079 m, with a length of 435 m. There was a warning sign located at 300 m upstream of the work zone and there was no posted work zone speed limit. The durations of green, yellow, and red phases were 25 s, 5 s, and 60 s, respectively. Characteristics of the studied road segment are listed in Table 1. The data used in this study was collected between December 9th and December 23rd of 2018 when the work zone was under construction. Two types of traffic data were collected: microscopic and macroscopic data. Macroscopic data include travel time, speed, and vehicle volume, which are accessible from the data collection system BlueTOAD installed on both ends of the road section. The system measures travel time and delay of travelers by detecting Bluetooth MAC addresses of passing devices (e.g., mobile phones, earphones and in-vehicle hand-free audio systems) and comparing the time of these addresses from one known location to another. Macroscopic data including average travel time, average traffic speed and traffic volume on the studied road segment were collected by BlueTOAD at a 15-min interval from 0:00 to 24:00 for 15 days. According to the field observation, the truck ratio is about 5%.

For the microscopic data collection, the video-photographic method is the most widely used technique. However, the method is not suitable in this study because many cameras are needed to cover long road sections and the accuracy is not guaranteed with fewer cameras. Therefore, a smartphone-based GPS method is used to collect the microscopic data of moving vehicles in this study. The instantaneous vehicle speed and trajectory were measured through a mobile app called GPS Speedometer installed on the drivers' smartphone and the mobile app has an accuracy of 98%. Vehicles moved in tandem along the road to consider the interaction between vehicles. The limitation of this method is that the data collection is restricted by the available resources, such as drivers, vehicles, and smartphones. In this study, during each round of data collection, two experienced test drivers were asked to drive through the whole road section from the beginning to the end, and the longitudinal trajectory and speed data of the two cars were collected with the mobile app at a 1-s interval. To reflect relatively realistic vehicle interaction in moderate traffic, the time gap between the two cars was controlled around 2 s. A total of 12 rounds of data collection were conducted.

Table 2
Calibrated parameters for the proposed model.

Parameters	Car	Truck
Vehicle length l (m)	6	12
Acceleration a (m/s^2)	1	0.5
Deceleration d (m/s^2)	1.5	1
Deceleration capability M (m/s^2)	4	3
Maximum velocity v_{max} (m/s)	18	15.5
Work zone speed limit v_r (m/s)	13.5	
Stochastic noise related parameter v_s (m/s)	5.5	
Randomization probability R_s	0.36	
Stopping probability related parameter α	0.17	
Stopping probability related parameter β (m)	55.5	

4.2. Model calibration

The proposed model is then calibrated with the collected data macroscopically and microscopically. Because microscopic data of trucks are not available, microscopic calibration is conducted for cars only. Parameters of trucks, such as vehicle length l, acceleration rate a, vehicle deceleration rate d, and deceleration capability M provided in Li et al. [7] are used, as shown in Table 1. Moreover, it is observed that maximum velocities for cars and trucks outside the work zone area are about 18 m/s (40 mph) and 15.5 m/s (35 mph), respectively. The observed maximum velocity in the work zone area for both vehicle types is about 13.5 m/s (30 mph). Preliminary tests show that some model parameters have more significant influence on the vehicle trajectory and speed than the rest, while others have greater influence on the macroscopic dynamics of traffic flow. Therefore, calibrations are performed in two steps. Firstly, 8 sets of trajectory and speed data are used to calibrate parameters of cars including the vehicle acceleration rate a, vehicle deceleration rate d, and deceleration capability M. Secondly, aggregated average travel speed data of the first 10 days are used to calibrate model parameters including the randomization probability R_s, the stopping probability-related parameter α and β, and the stochastic noise-related parameter v_s. Following the work by Cunha et al. [31], a genetic algorithm coded in Matlab® is used in the macroscopic and microscopic calibration, and the calibrated parameter values for the proposed model are found and displayed in Table 2.

4.3. Model validation

The validation of the proposed model is conducted at microscopic and macroscopic levels. In microscopic validation, we compared the trajectory and speed of individual vehicles generated from the proposed model with the measured field data. In macroscopic validation, the simulated average travel speeds were compared with the measured field data.

4.3.1. Microscopic validation

The proposed model is firstly validated with the rest 4 sets of measured trajectory and speed data. To generate the same initial headway, observed vehicle arrival distribution and entry speed are used to generate vehicles in the simulation. Fig. 3 shows the comparison of the observed and simulated longitudinal trajectories and speeds for two cars. It can be seen from the figure that both cars decelerate from the maximum velocity before entering the work zone, accelerate after leaving the work zone, and stop in front of the red traffic light finally. There is good agreement between the simulated trajectory and speed and the field data for both cars. However, relatively large speed deviations are found in the work zone area (Fig. 3b), especially for car 2, due to the stochastic characteristic of traffic dynamics. This indicates that microscopic traffic dynamic is not only affected by the vehicle performance, but also the driving behaviors of different drivers, especially in abnormal driving environments such as disrupted roadways. Moreover, some obvious trajectory deviations are found for car 2 when it approached the traffic light (Fig. 3a), which was mainly resulted from the speed deviations in the work zone area.

Error tests are used to quantitatively evaluate the performance of the proposed model. The overall error between the simulation results and field data are quantified by the root mean square percent error (RMSE) and mean percent error (MPE). The equations of RMSE and MPE can be expressed as follows.

$$RMSE = \sqrt{\frac{1}{N}\sum_{k=1}^{N}\left(\frac{\hat{z}_k - z_k}{z_k}\right)^2} \tag{25}$$

$$MPE = \frac{1}{N}\sum_{k=1}^{N}\left(\frac{\left|\hat{z}_k - z_k\right|}{z_k}\right) \tag{26}$$

where $\hat{z}_k$ is the simulated value from the proposed model, z_k is the corresponding observed value from the field data, and N is the number of observations. Error tests are performed for the trajectories and speeds of each vehicle at each second.

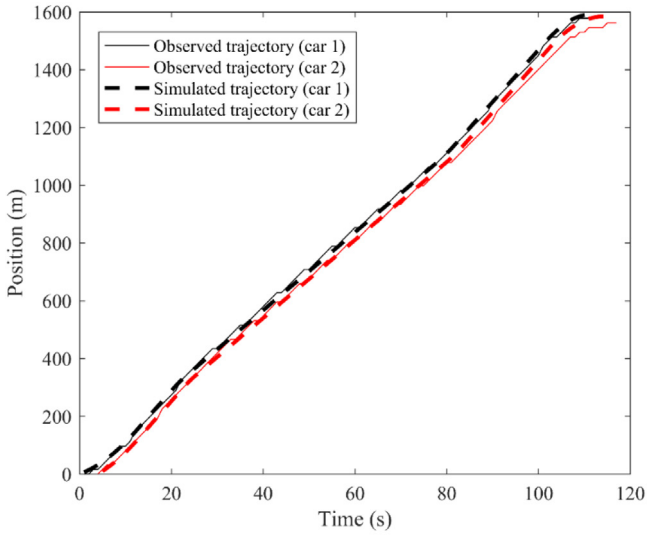

(a) Position

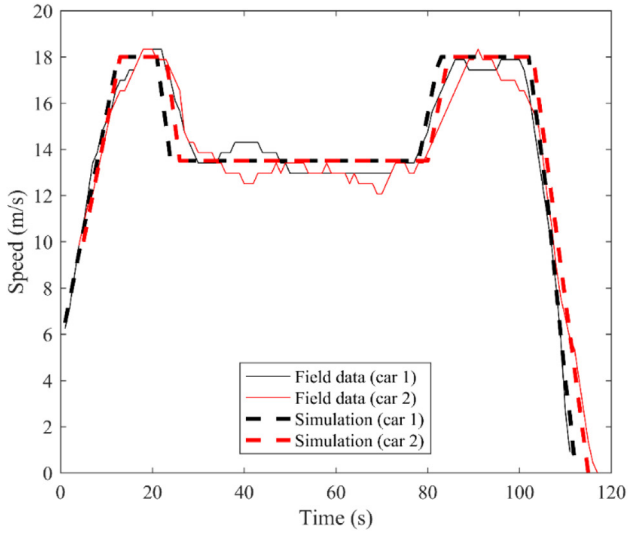

(b) Speed

Fig. 3. Comparison between observation and CA simulation.

According to the error tests result, the RMSE and MPE of the vehicle trajectories are less than 7% and 4%, respectively. The RMSE and MPE of vehicle speeds are less than 7% and 6%, respectively. The deviations between the simulation and field data are relatively small and deemed acceptable. Therefore, we can conclude that the proposed model can capture the traffic dynamics of disrupted flow at the microscopic level with reasonable accuracy.

4.3.2. Macroscopic validation

The model is then validated with average travel speed data from the rest 5 days of the 15 days. Firstly, the speed–volume relationship from the simulation results was compared with the field data. Fig. 4 shows the comparison of the speed–volume relationships from both field data and simulation. It can be seen from the figure that the simulated speed–volume relationship has generally good agreement with the observed field data. Relatively large discrepancy under moderate traffic conditions possibly results from the stochasticity and instability of urban traffic flow. Secondly, we

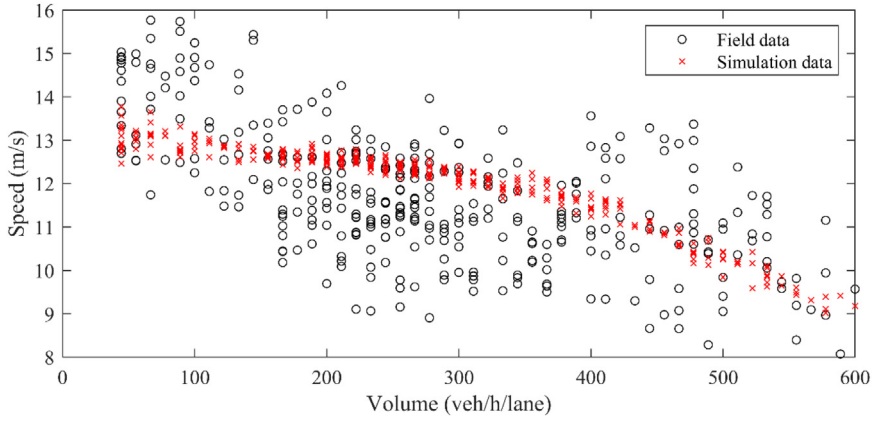

Fig. 4. Comparison of speed–volume relationship from field data and simulation.

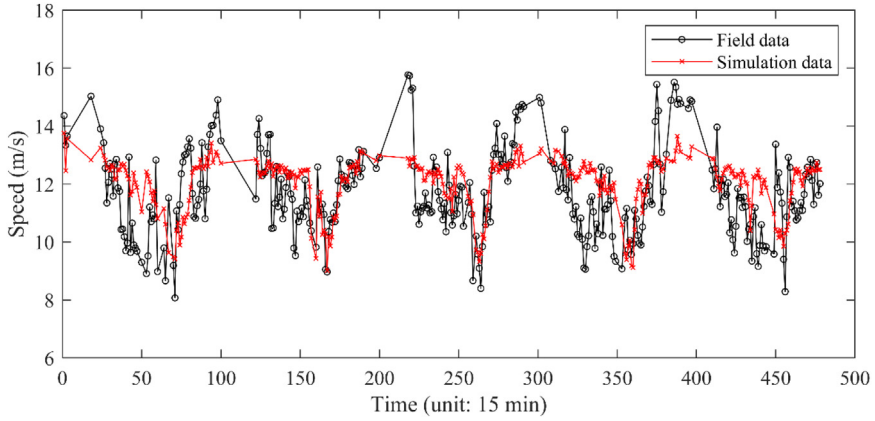

Fig. 5. Comparison of time series of speed from field data and simulation.

compared the simulated time series of speed with field data to evaluate how well the proposed model performs in the time domain. Fig. 5 shows the comparison of time series of speed from field data and simulation. It is found that the simulated speeds match well with the field data in general, although there is relatively large discrepancy during some periods (e.g., 11 am to 1 pm) when the traffic is very unstable. RMSE and MPE are still used for the overall error of the aggregated speed between simulation results and field data, which are found to be 12% and 9%, respectively. These errors are within the acceptable limit as stated by Meng and Weng [24] for the CA-based model in terms of travel speed. These results show that the proposed model can realistically reproduce the disrupted traffic flow at the macroscopic level.

5. Development of travel time functions for PBR

5.1. Simulation experiments

Demand flow rate, truck ratio and blockage ratio are identified as the three key factors that affect travel time in past studies. It is noted that the demand flow exclusively denotes vehicles entering the PBR at the upstream entry and the demand flow rate is equal to the flow rate of q in Section 3.2. When the demand flow rate is higher than the capacity of the PBR, an oversaturated traffic is formed. Blockage ratio is defined in this study as the ratio between the length of the blockage and the total length of the road. To quantitatively evaluate the influence of demand flow rate, truck ratio and blockage ratio on travel time, microscopic simulation experiments are conducted with the validated model on the same disrupted road in the last section. A total of 525 combination scenarios for 15 demand flow rates (50 to 750 veh/h/lane with a 50 veh/h/lane increment), 7 truck ratios (0% to 30% with a 5% increment) and 5 blockage ratios (10% to 50% with a 10% increment) are simulated.

Fig. 6 shows the simulated travel time–volume data with different truck ratios when the blockage ratio R_b equals 30%. Fig. 7 shows the simulated travel time–volume data with different blockage ratios when the truck ratio R_t equals 20%. Several general observations can be made from the simulation results in Figs. 6 and 7. Firstly, the travel time increases as

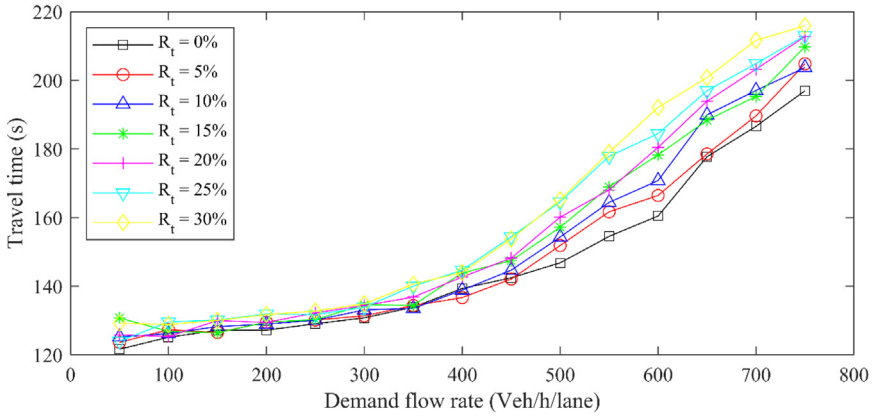

Fig. 6. Simulated travel time-demand flow rate data with different truck ratios ($R_b = 30\%$).

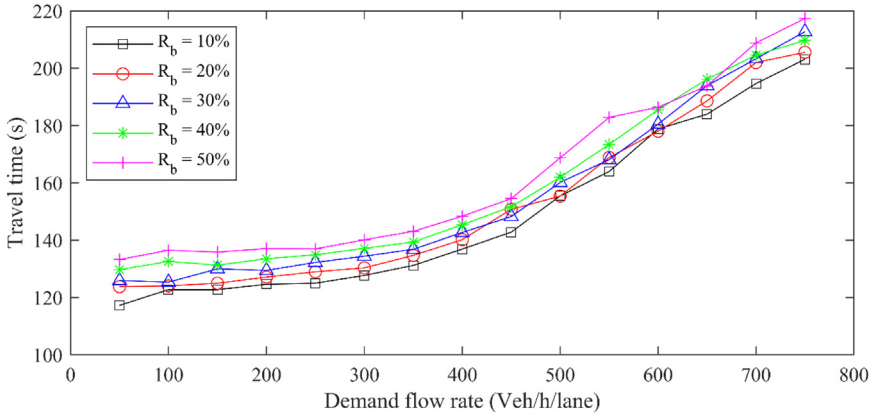

Fig. 7. Simulated travel time-demand flow rate data with different blockage ratios ($R_t = 20\%$).

the demand flow rate increases. Secondly, it is found in Fig. 6 that the travel time increases as the truck ratio increases and the impact of the truck ratio becomes more significant when the demand flow rate is higher. Thirdly, it can be found in Fig. 7 that the travel time increases with the increase of the blockage ratio. However, as the demand flow rate increases, the influence of the blockage ratio becomes slightly less significant.

5.2. Regression analysis of travel time functions

To consider the effect of trucks on the travel time–volume relationship, Yun et al. [10] proposed a revised BPR function, which has the following form.

$$t = t_0 \left[1 + \alpha \, (1 + R_t)^{\beta} \, (f/C)^{\gamma}\right] \tag{27}$$

where t is the travel time; t_0 is the free-flow time; f is the demand flow rate; C is the road capacity; α, β and γ are coefficients. The term $(1 + R_t)^{\beta}$ in Eq. (27) is used to reflect the impact of the truck ratio on the travel time in a reasonable way. Firstly, the value of this term becomes 1 when the truck ratio $R_t = 0$. This ensures that Eq. (27) is consistent with the BPR function. Secondly, the value of $(1 + R_t)^{\beta}$ increases as the truck ratio R_t increases when $\beta > 0$.

As discussed earlier, the blockage ratio R_b has following effects on travel time: a significant increase in the free-flow time as R_b increases, and less significant influence when the demand flow rate is higher. Therefore, two modifications of Eq. (27) need to be made to consider the effect of the blockage ratio. Firstly, a new term $f(R_b)$, which is a function of the blockage ratio R_b, is introduced to replace the constant free-flow time t_0. This ensures that different blockage ratios correspond to different free-flow time. Several possible function forms (e.g., linear, quadratic, exponential functions) are tested, and it is found that a simple linear function can provide a very good fit of the observed data. Secondly, a power function in the form of $(1 + R_b)^{\beta}$ is introduced to consider the decreasing effect of the blockage ratio with the increase of the demand flow rate. When $\beta < 0$, the value of $(1 + R_b)^{\beta}$ decreases as the blockage ratio R_b increases. The other reason

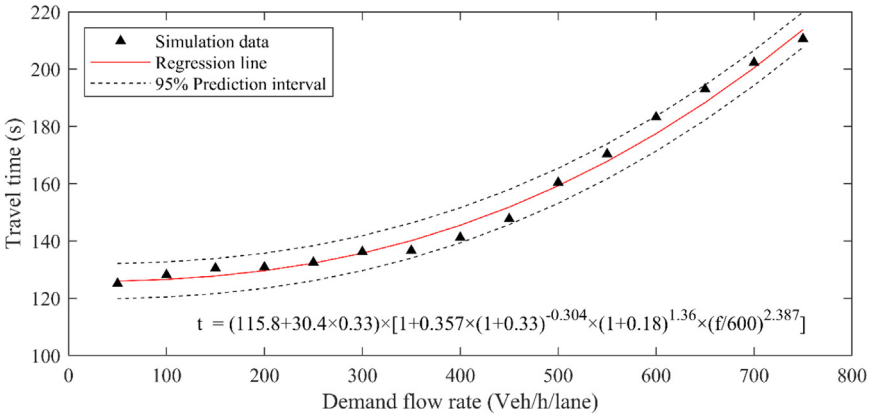

Fig. 8. Validation results for a random selected scenario ($R_b = 0.33$ and $R_t = 0.18$).

that we choose the power function is that it has a consistent form as the term about the truck ratio R_t, which allows for easy calibration. Finally, the modified travel time function has the following form:

$$t = (\alpha_1 + \alpha_2 R_b)\left[1 + \alpha_3 (1 + R_b)^{\alpha_4} (1 + R_t)^{\alpha_5} (f/C)^{\alpha_6}\right] \tag{28}$$

where α_1, α_2, α_3, α_4, α_5, and α_6 are parameters.

A nonlinear regression analysis is performed to estimate the parameters of the travel time function shown in Eq. (28) with the simulated 525 data sets. The road capacity used in the analysis is determined based on the speed–volume relationship from the field data, which is around 600 vehicle/h/lane. The calibrated travel time functions are shown as follows.

$$t = (115.8 + 30.4 R_b)\left[1 + 0.357 (1 + R_b)^{-0.304} (1 + R_t)^{1.36} (f/C)^{2.387}\right] \tag{29}$$

To measure how well the regression model describes the simulated data, the goodness-of-fit statistics are evaluated. The high value of R^2 (0.99) clearly indicates that the calibrated travel time functions can capture the relationship between the travel time and the demand flow rate, truck ratio and blockage ratio very well. The high value of F (41815) also indicates overall significance of the regression model.

The calibrated travel time functions are further validated by predicting the travel time of the random traffic scenarios and comparing them against the actual values. A randomly selected scenario ($R_b = 0.33$ and $R_t = 0.18$) that was not included in the previous simulation is used in the validation analysis. The validation results are shown in Fig. 8, from which all new simulation data of the selected scenario falls in the 95% prediction intervals of the regression travel time. Similar validation results are also obtained for other random scenarios, and this indicates that the calibrated travel time functions can predict new observations with acceptable accuracy.

5.3. Discussion on the application of travel time function for PBR

Accurate estimation of travel time on PBR is very important for the performance assessment of post-hazard transportation networks. However, the standard BPR function was usually used in the past for travel time prediction on PBR in the post-hazard transportation demand modeling, due to the unavailability of travel time functions derived specifically for PBR. In this section, we will compare the developed travel time functions with the standard BPR function to identify the difference between them. The comparison of the calibrated travel time functions of different traffic scenarios and the standard BPR function for PBR is shown in Fig. 9. There are 6 different combination scenarios in Fig. 9, including 3 blockage ratios and 2 truck ratios. In line with previous practice, the free-flow time under normal condition ($t_0 = 109$ s) and the reduced traffic capacity ($C = 600$ Veh/h/lane) are substituted into the standard BPR function, $t = t_0\left(1 + 0.15\,(f/C)^4\right)$, to get the travel time function.

Several limitations of the standard BPR function can be identified from Fig. 9. Firstly, since there is only one curve for the standard BPR function, it cannot consider the difference between different traffic scenarios with different vehicle compositions and blockage sizes. Secondly, the curve of the standard BPR is considerably different from that of the calibrated functions. Although the values from both functions increase over demand-to-capacity ratio, the increment is much smaller under undersaturated condition for the standard BPR function, because the interaction between vehicles and the obstruction was not considered. Thirdly, the standard BPR function underestimates the travel time under both undersaturated and oversaturated conditions as compared to the calibrated functions. For example, for the scenario where the blockage ratio $R_b = 10\%$ and truck ratio $R_t = 10\%$, the estimated travel time by the standard BPR function is 25% lower when the demand-to-capacity ratio is 1.0. Underestimation of travel time with the standard BPR function will

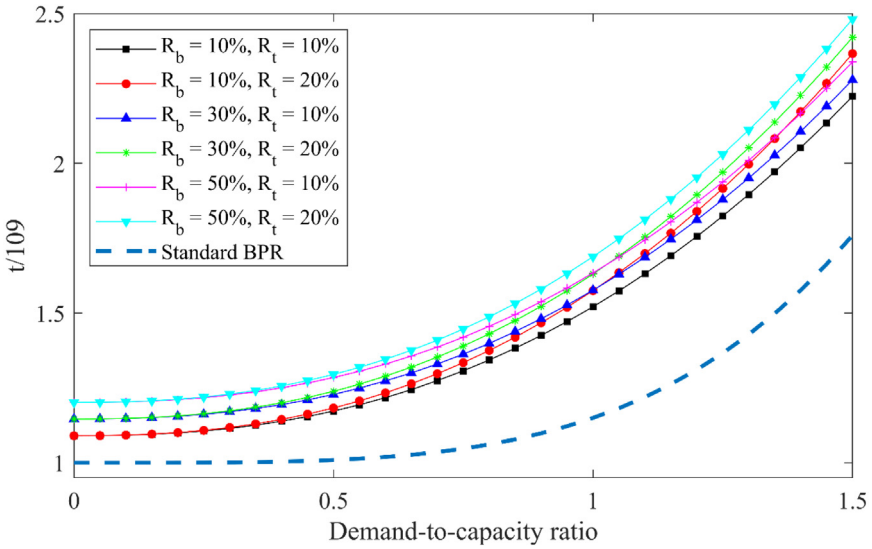

Fig. 9. Comparison of calibrated travel time functions and standard BPR function.

lead to biased travel demand estimates. Apparently, the calibrated travel time functions can give more realistic travel time prediction over the standard BPR function, which in turn leads to realistic travel demand estimate in post-hazard transportation network analysis.

6. Conclusions

By overcoming the limitations of previous studies, we have, for the first time, established the methodology of developing the travel time functions of PBR in urban areas and studied the feasibility of developing such functions by calibration and validations with the field data. Firstly, an improved CA model was proposed for heterogeneous traffic flow on partially blocked arterial roads by extending the two-lane SD model. With the proposed model, two types of unrealistic deceleration behaviors in most existing CA models can be avoided. Meanwhile, driver's behaviors during traffic signal change intervals were realistically replicated by determining the vehicle status based on the vehicle's distance to the intersection, driving speed and stopping probability. Secondly, the proposed model was calibrated and validated with the collected field traffic data in both macroscopic and microscopic scales. The validation results show that the proposed model can simulate the disrupted traffic flow with acceptable accuracy. Finally, the traffic data under various scenarios with different demand flow rates, truck ratios and blockage ratios were generated through microscopic simulation experiments. The experiment results demonstrate that both blockage ratio and truck ratio have significant influence on the travel time. A continuous traffic time function was proposed for the disrupted traffic flow to capture the effect of the blockage ratio and truck ratio on the travel time. Its parameters were then estimated through a nonlinear regression analysis with the generated traffic data. Comparison results show that the developed travel time functions can provide more flexible and accurate predictions of travel time for PBR than the standard BPR function.

Like the traditional BPR function, new travel time functions that are intended for practical use should be extensively validated with field data from sites with varying supply and demand conditions (e.g., road classes, signal settings at downstream intersection). Because there is no sufficient and reliable traffic data of partially blocked roads at this point, the proposed travel time functions in this study are calibrated and validated with field data from a single site. Therefore, this study does not aim to propose a universal and practice-ready travel time function, rather develop the simulation-based methodology and study the feasibility of developing such travel time functions for PBR once sufficient traffic data becomes available in the future. This study also has some limitations: (1) the impact of the relative location of the blocked area is not investigated in this study. Although the proposed methodology can simulate different relative locations of the blocked areas, large amount of field data set is needed to calibrate and validate the simulation results. Due to the scarcity of the traffic data on disrupted roads, this can be an important topic which will be explored in the future; (2) due to the scope limit, the signal setting of the downstream intersections was not studied. As the future study, traffic signal designs of typical intersections can be incorporated by extending the proposed methodology.

There are many potential applications and future studies based on the proposed methodology. For example, developed travel time functions of PBR can be used to accurately predict the traffic demand of post-hazard transportation networks with disrupted roads, and further help enhance transportation network resilience. Besides, travel time functions of PBR can be employed to develop effective work zone management plans by estimating negative impacts of work zones on traffic mobility in the network level.

CRediT authorship contribution statement

Guangyang Hou: Conceptualization, Methodology, Software, Validation, Formal analysis, Investigation, Data curation, Writing – original draft. **Suren Chen:** Conceptualization, Supervision, Project administration, Funding acquisition, Writing – review & editing. **Yulong Bao:** Investigation.

Declaration of competing interest

The authors declare that they have no known competing financial interests or personal relationships that could have appeared to influence the work reported in this paper.

Acknowledgments

The authors gratefully acknowledge the support of this research by the United States Department of Transportation (through the Mountain Plains Consortium) and the Center for Risk-based Community Resilience sponsored by National Institute of Standards and Technology (NIST), USA (Award No. 70NANB15H044). The authors would also like to thank the Traffic Operations Department in the City of Fort Collins for sharing the traffic monitoring data. Any opinions, findings, and conclusions expressed in this material are those of the investigators and do not necessarily reflect the views of the sponsors.

References

[1] Bureau of Public Roads, Traffic Assignment Manual, U.S. Dept. of Commerce, Urban Planning Division, Washington D.C, 1964.
[2] H. Spiess, Conical volume-delay functions, Transp. Sci. 24 (1990) 153–158.
[3] R. Akcelik, Travel time functions for transport planning purposes: Davidson's function, in: Its Time Dependent Form and Alternative Travel Time Function, Vol. 21, Australian Road Research, 1991.
[4] C. Xie, R.L. Cheu, D.H. Lee, Calibration-free arterial link speed estimation model using loop data, J. Transp. Eng-Asce 127 (2001) 507–514.
[5] A. Skabardonis, R. Dowling, Improved speed-flow relationships for planning applications, Transp. Res. Rec.: J. Transp. Res. Board (1997) 18–23.
[6] Highway capacity manual, in: Transportation Research Board, National Research Council, Washington D.C, 2000.
[7] X. Li, X.G. Li, Y. Xiao, B. Jia, Modeling mechanical restriction differences between car and heavy truck in two-lane cellular automata traffic flow model, Physica A 451 (2016) 49–62.
[8] Z.Y. Lu, Q. Meng, G. Gomes, Estimating link travel time functions for heterogeneous traffic flows on freeways, J. Adv. Transp. 50 (2016) 1683–1698.
[9] S. Muller, C. Schiller, Improvement of the volume-delay function by incorporating the impact of trucks on traffic flow, Transp. Plan. Tech. 38 (2015) 878–888.
[10] S. Yun, W.W. White, D.R. Lamb, Y.Q. Wu, Accounting for the impact of heavy truck traffic in volume-delay functions in transportation planning models, Plan. Anal. 2005 (2005) 8–17.
[11] H. Adeli, X.M. Jiang, Neuro-fuzzy logic model for freeway work zone capacity estimation, J. Transp. Eng-Asce 129 (2003) 484–493.
[12] M.J. Cassidy, L.D. Han, Proposed model for predicting motorist delays at 2-lane highway work zones, J. Transp. Eng-Asce 119 (1993) 27–42.
[13] S. Argyroudis, J. Selva, P. Gehl, K. Pitilakis, Systemic seismic risk assessment of road networks considering interactions with the built environment, Comput-Aided Civ. Inf. 30 (2015) 524–540.
[14] A. Goretti, V. Sarli, Road network and damaged buildings in urban areas: Short and long-term interaction, B Earthq. Eng. 4 (2006) 159–175.
[15] M.A. Zanini, F. Faleschini, P. Zampieri, C. Pellegrino, G. Gecchele, M. Gastaldi, R. Rossi, Post-quake urban road network functionality assessment for seismic emergency management in historical centres, Struct. Infrastruct. E 13 (2017) 1117–1129.
[16] U. Tamima, L. Chouinard, Systemic seismic vulnerability of transportation networks and emergency facilities, J. Infrastruct. Syst. 23 (2017).
[17] G. Hou, S. Chen, Y. Zhou, J. Wu, Framework of microscopic traffic flow simulation on highway infrastructure system under hazardous driving conditions, Sustain. Resil. Infrastruct. 2 (2017) 136–152.
[18] L. Fei, H.B. Zhu, X.L. Han, Analysis of traffic congestion induced by the work zone, Physica A 450 (2016) 497–505.
[19] G.Y. Hou, S.R. Chen, Y. Han, Traffic performance assessment methodology of degraded roadway links following hazards, J. Aerospace Eng. 32 (2019).
[20] G. Hou, S. Chen, Study of work zone traffic safety under adverse driving conditions with a microscopic traffic simulation approach, Accid. Anal. Prev. 145 (2020) 105698.
[21] D.W. Huang, W.N. Huang, The influence of tollbooths on highway traffic, Physica A 312 (2002) 597–608.
[22] B. Jia, R. Jiang, Q.-S. Wu, The traffic bottleneck effects caused by the lane closing in the cellular automata model, Internat. J. Modern Phys. C 14 (2003) 1295–1303.
[23] S. Kurata, T. Nagatani, Spatio-temporal dynamics of jams in two-lane traffic flow with a blockage, Physica A 318 (2003) 537–550.
[24] Q. Meng, J.X. Weng, An improved cellular automata model for heterogeneous work zone traffic, Transp. Res. C-Emer 19 (2011) 1263–1275.
[25] K. Nassab, M. Schreckenberg, A. Boulmakoul, S. Ouaskit, Effect of the lane reduction in the cellular automata models applied to the two-lane traffic, Physica A 369 (2006) 841–852.
[26] A. Pottmeier, R. Barlovic, W. Knospe, A. Schadschneider, M. Schreckenberg, Localized defects in a cellular automaton model for traffic flow with phase separation, Physica A 308 (2002) 471–482.
[27] H.B. Zhu, L. Lei, S.Q. Dai, Two-lane traffic simulations with a blockage induced by an accident car, Physica A 388 (2009) 2903–2910.
[28] L.W. Lan, Y.C. Chiou, Z.S. Lin, C.C. Hsu, A refined cellular automaton model to rectify impractical vehicular movement behavior, Physica A 388 (2009) 3917–3930.
[29] M.E. Larraga, L. Alvarez-Icaza, Cellular automaton model for traffic flow based on safe driving policies and human reactions, Physica A 389 (2010) 5425–5438.
[30] C.C. Hsu, Y.C. Chiou, A modified cellular automaton model for accounting for traffic behaviors during signal change intervals, J. Adv. Transp. (2018).
[31] A.L. Cunha, J.E. Bessa, J.R. Setti, Genetic algorithm for the calibration of vehicle performance models of microscopic traffic simulators, in: Portuguese Conference on Artificial Intelligence, Springer, 2009, pp. 3–14.